Materials Research Express

PAPER

Room temperature electrical properties and excitation performance of Al_2O_3 doped fused silica ceramics

To cite this article: Sugato Hajra *et al* 2019 *Mater. Res. Express* **6** 126325

Materials Research Express

PAPER

Room temperature electrical properties and excitation performance of Al_2O_3 doped fused silica ceramics

Sugato Hajra[1], **Manisha Sahu**[1], **Varsa Purohit**[1], **Kalyani Mohanta**[2], **Basanta K Panigrahi**[1] and **P L Deepti**[3]

[1] Institute of Technical Education and Research, Siksha O Anusandhan (Deemed to be University), Bhubaneswar-751030, India
[2] Department of Ceramic Engineering, Indian Institute of Technology- BHU, Varanasi-221005, India
[3] Department of Physics, Veer Surendra Sai University of Technology, Burla-768018, India

E-mail: sugato.hazra.sjc@gmail.com

RECEIVED
9 October 2019

REVISED
30 November 2019

ACCEPTED FOR PUBLICATION
20 December 2019

PUBLISHED
8 January 2020

Keywords: dielectric, silica, impedance, conductivity

Abstract

Al_2O_3 doped fused silica ceramic samples were synthesized by colloidal processing route. X-ray diffraction technique helped to give insight upon the phase formation of the synthesized samples. The dense growth of grains was depicted from surface micrographs. The frequency-dependent electrical properties of both sintered and quenched samples were examined from 100 Hz till 1 MHz. The frequency-dependent AC conductivity followed Jonscher's power law. The dielectric relaxation and Nyquist plot confirm the non-Debye nature in both sintered as well as quenched samples. The ferroelectric properties were depicted in the prepared samples. The sintered and quenched Al_2O_3 doped fused silica samples reveals that the samples get excited on the application of electric field and further can be utilized in filter application.

1. Introduction

The lead-based ceramics have superior properties and share its role in development of technological appliances since past decades [1–3]. Particularly in miniaturization of electronic devices such as transistors and memories are influenced by shape/interface control. However, the underlying mechanisms are inconsistent due to scarcity of synthesis route, characterization process and functionalization strategy. It is observed that there is an urge to fabricate lead free ceramics with similar properties acting as an alternative base for device engineering. The strict measures undertaken by world legislation have forced the industries to manufacture lead free electronics keeping into view the global environmental hazards caused by toxicity of lead [4, 5]. Fused silica ceramics have excellent thermal shock resistance, low coefficient of thermal expansion and dielectric parameters (dielectric constant 3.1–3.8, dielectric loss 0.0004) [6]. Alumina is preferred additive for silica-based ceramics. The impurity of alumina is present in fused silica raw powders and its extraction is costly, especially during high purity fused silica powders processing. However, the alumina as a dopant in fused silica ceramics and its effect on physical properties has been examined in less detail. The processing route plays a vital role in controlling the detailed mechanism of Al_2O_3 doped fused silica ceramics. The colloidal processing route is preferred over the convention dry pressing route due to enhancement in homogeneity with improved packing reducing the sintering temperature [7]. The same authors have reported the dielectric and impedance analysis on the fused silica ceramics [8].

However, after surveying the past literature we see that no consistent results on the dielectric relaxation and conduction mechanism have been reported on Al_2O_3 doped fused silica samples. In this context, the authors examine the comparison study of structure, micro-structure and electrical properties of sintered as well as quenched Al_2O_3 doped fused silica samples. Further attempt has been made to realize the excitation performance of the prepared samples by applying an electric field.

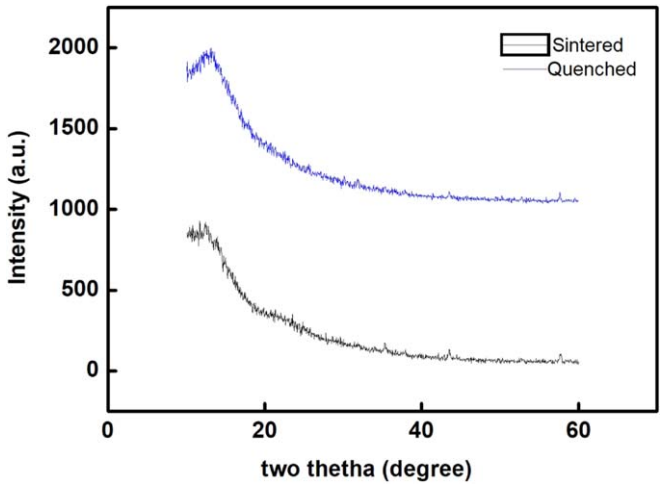

Figure 1. XRD pattern of sintered (black) and quenched (blue) at room temperature.

2. Processing and experimental techniques

The samples were generated using colloidal processing route with help of fused silica powder (M/S Chettinad Fused quartz Pvt. Ltd, India) and alumina powder (M/S Alcoa-*USA)*. The binder employed during formation of suspension was extract of fresh eggs (egg white) and sucrose. Further, magnetic stirrer helped in homogenization of egg white which was continued for 2 h. The egg white or sucrose was blended along with various quantity of distilled water helping towards processing of Al_2O_3 doped fused silica. In a polypropylene bottle the suspension was taken as 55–70 vol% of suspensions and 3 mm zirconia subjected to roll milling for 24 h. The 1-octanol (5 ml) was introduce to reduce the bubble formation during the making of slurry. The zirconia media are drain from slurry after milling carried for 24 h, and various measurements were conducted. The prepared slurry was poured into aluminium molds of rectangular shape and grease like lubricant was applied before pouring the slurry. Then annealing took place at 60 °C for 24 h. The green parts were removed from mold at room temperature, and further annealed for 24 h. The prepared samples were fired at 900 °C for 2 h to remove the organics and gain handling strength. Finally, sintering was executed at 1100 °C and soaking period of 2 h. The thermal cycling for 5 times was performed for as sintered Al_2O_3 substituted fused silica samples. A single thermal cycle involves 900 °C heating, a 30-minute dwell at 900 °C after that quenching in chilled water (5 °C).

The structural evaluation of the prepared samples was examined by powder x-ray diffractometer of Rigaku with CuK_α radiation ($\lambda = 1.5405$) and 2θ ($20 \leqslant 2\theta \leqslant 80^o$). The surface micrograph was recorded by FEI Nova nanoSEM 600. The various electrical properties were recorded using LCR meter keeping frequency sweep from 1 kHz to 1 MHz at room temperature. Before electrical measurements one pellet of each composition was smoothed at both sides and painted with highly conductive silver paint. The annealing of the pellets at 120 °C for 3 h helped to remove moisture. The hysteresis loops (polarization versus electric field) was recorded using ferroelectric loop tracer (M/S Marine India).

3. Results and discussion

3.1. Structural and morphology

Figure 1 shows the structural information of the sintered (represented by black colour) and quenched (represented by blue colour) samples. The formation of dispersed cristobalite takes place beyond 1100°C during fused silica processing. Hence at 1100 °C, the formation of the prepared samples is confirmed as no cristobalite phase is seen. Figures 2(a), (b) inset presents the surface micrographs for both the sintered and quenched samples suggests that there is a densely packed grain throughout. The elemental analysis confirms the presence of all the elements like Si, Al, O in figures 2(a), (b). The mapping results depicts that the both sintered and quenched samples are synthesized with no impurities. The elemental atomic ratio of each element is calculated from EDAX spectra data are presented in table 1 (sintered) and table 2 (quenched).

3.2. Dielectric properties

The room temperature data of dielectric constant and tan δ of the sintered (represented by black colour) and quenched (represented by red colour) in figures 3(a), (b) specimens are shown with respect to wide frequency

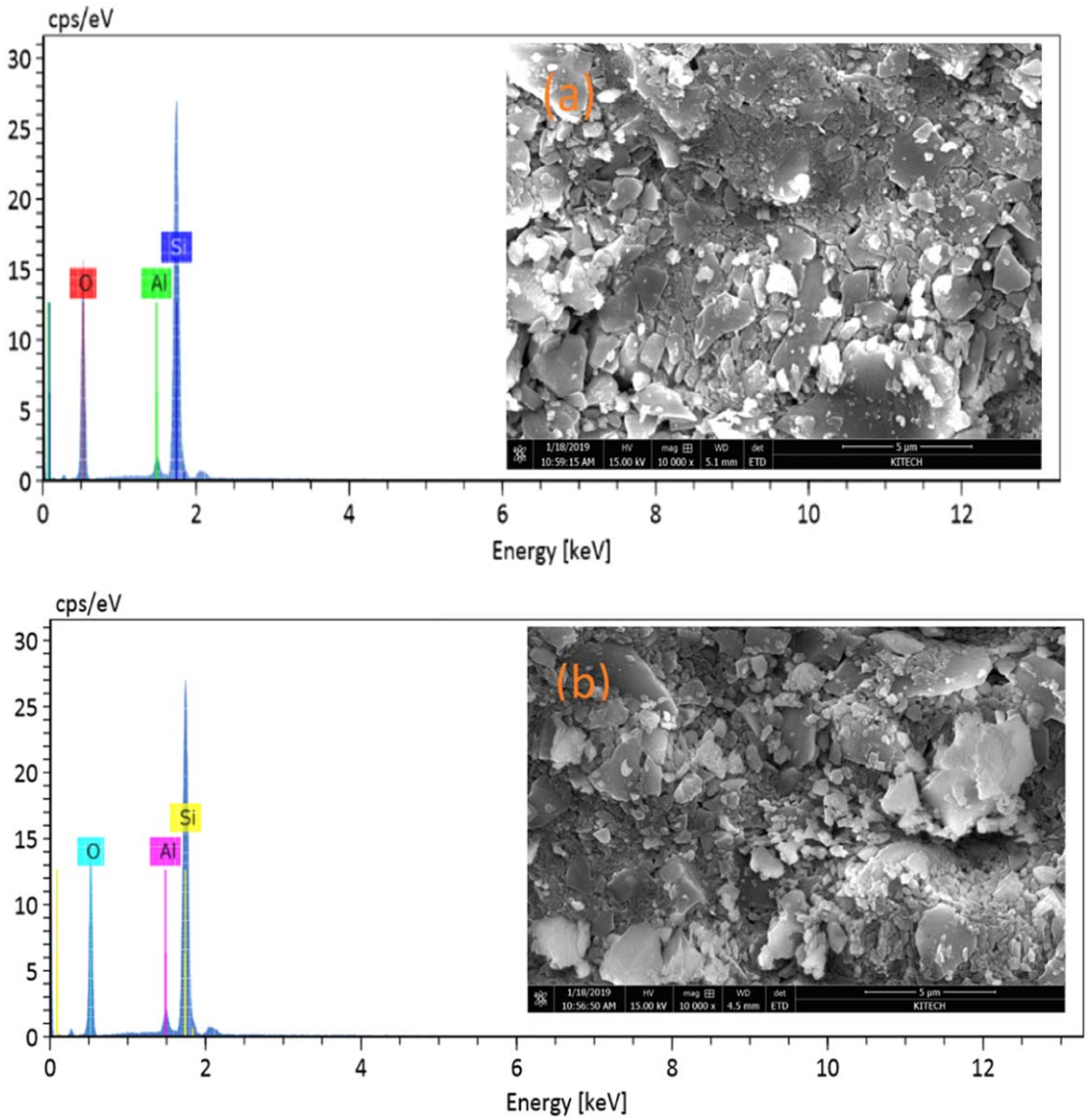

Figure 2. Inset shows surface micrograph and compositional analysis of the (a) sintered and (b) quenched sample.

Table 1. Element, wt%, at%, and elemental atomic ratio for sintered sample.

Element	Wt%	At%	Elemental atomic ratio O/(Si+Al)
Al	2.39	1.78	0.052
Si	45.05	32.22	0.947
O	52.56	66.00	1.941

Table 2. Element, wt%, at%, and elemental atomic ratio for quenched sample.

Element	Wt%	At%	Elemental atomic ratio O/(Si+Al)
Al	2.97	2.24	0.061
Si	46.81	33.91	0.938
O	50.22	63.85	1.766

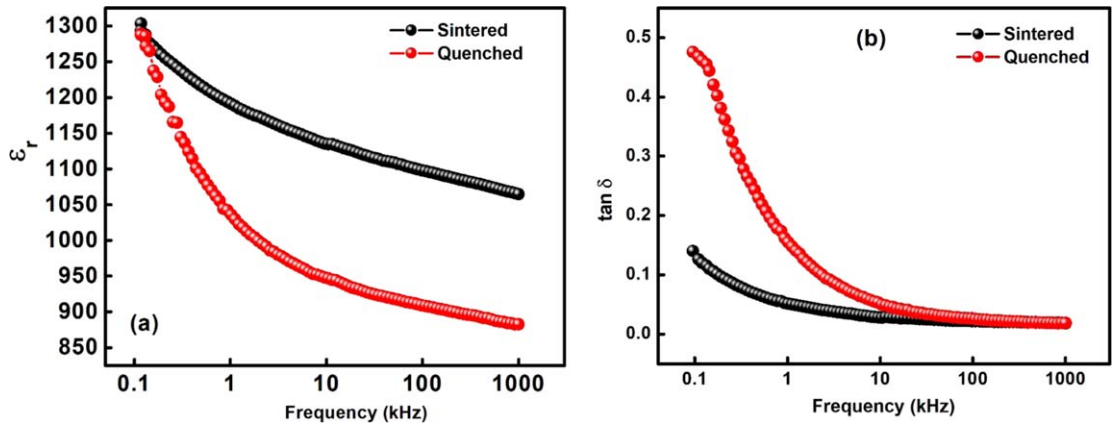

Figure 3. Frequency dependent dielectric constant (a) and loss tangent (b) of sintered (black) and quenched(red) samples at room temperature.

range. As noticed in the figure 3(a), both the samples obtain high dielectric constant at lower frequency. Application of electric field, structural deformation and thermal cycling during synthesis influence the dielectric parameters [9]. At lower frequency the dielectric value is large, afterward it decreases rapidly up to certain value of dielectric constant. The observed manners have been described by the dipolar relaxation phenomenon where at lower frequencies the dipoles follow the applied field frequency while at high frequencies dipoles are unable to follow the applied field [10]. As our compound is fabricated in colloidal slurry method, pores, voids, interstitials, vacancy defects, dislocations, dipoles are expected to contribute the complex dielectric constant of our sample. The several models such as Koop's phenomenological and Maxwell -Wagner shed gives idea about the dielectric constant dispersion. This phenomenological model suggests that grains and grain boundaries form the dielectric structure of ceramic compound. The conducting nature is shown for grains while grain boundaries are weakly conducting. In the region of high frequency, the grains are more active while in low-frequency region the grain boundaries contribution is dominant. There is accumulation of electrons and space charge polarization causing the grain boundaries to generate larger resistance. Consequently, at low frequencies the value of dielectric constant increases. As frequency of the electric field rise, the electrons movement vary their direction. It hinders the electrons motion, and further charges accumulation at the grain boundaries reduces, which decreases dielectric constant. The dielectric loss plot of the samples is shown in figure 3(b). The cause behind the higher dissipation may be due to high electric conductivity leading to rise of leakage current. High dissipation values at low frequencies are considered as resonance of the charge defect dipoles [11]. Generally, energy dissipations of sintered sample are less than the quenched one. It is depicted that the dissipation factor of sintered samples has low dielectric loss as compared to quenched samples. The reduction in loss factor suggest the insulation properties rise, which would have considerable potential for device application.

3.3. Electrical conductivity

Generally, when the external electric field is applied, the temperature dependent electrical conduction occurs in the dielectric specimens. The thermally activated charge carriers usually control the conduction process. The study of conductivity(electrical) of a ferroelectric material is essential as the associated properties like piezoelectricity, etc are reliant on it [12, 13].

Figure 4 illustrates ac electrical conductivity (σ_{ac}) change of (a) sintered and (b) quenched with respect of frequency at room temperature. The A C electrical conductivity is calculated using dielectric parameters as $\sigma_{ac} = 2\pi f \tan\delta\, \varepsilon_r \varepsilon_o$ where f = frequency of the applied field, tan δ = loss factor, ε_o = permittivity in free space [14]. The plot suggests that the conductivity is strongly frequency dependent.

Usually, the conductivity contains DC conductivity (frequency independent) and AC conductivity (frequency dependent) parts. This can be described using Jonscher's power law [15].

$$\sigma_{total}(\omega) = \sigma_{dc} + \sigma_{ac}(\omega) = \sigma_{dc} + A\omega^n$$

Here σ_{dc} = DC conductivity, $\sigma_{ac}(\omega)$ = AC conductivity, Here ω = angular frequency, A = a temperature dependent constant which denotes polarizability strength, n = temperature dependent exponent and $1 > n > 0$ [16].

According to Jonscher, the frequency-dependence of conductivity origin lies in the relaxation phenomena arising due to mobile charge carriers. When a mobile charge carrier hops to a new site from its original site, it remains in a state of displacement between two potential energy minima. Also, the conduction behaviour of

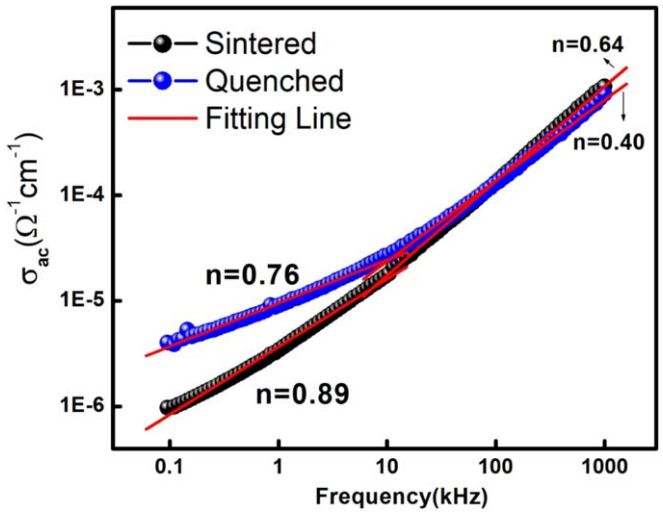

Figure 4. The variation of ac electrical conductivity (σ_{ac}) of sintered (black) and quenched (blue) samples with respect of frequency at room temperature and red line represents the fitting line.

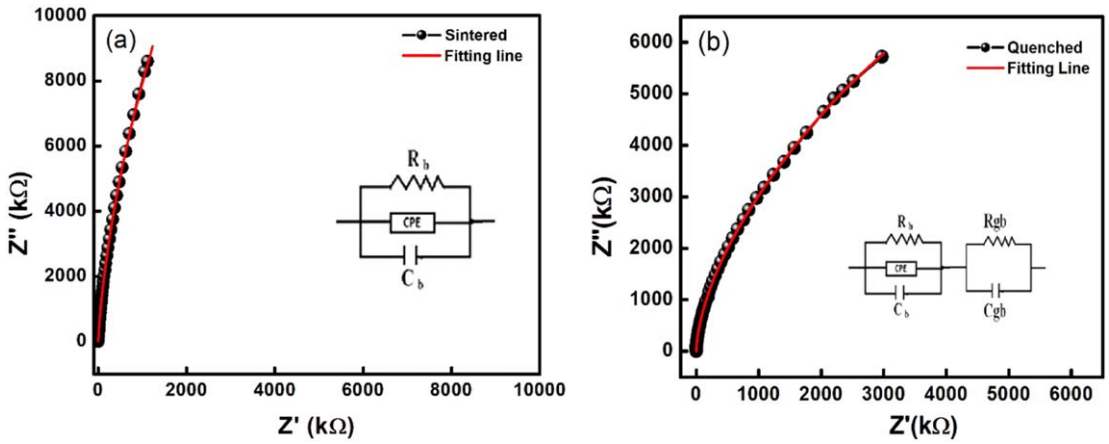

Figure 5. Nyquist Plot of (a) sintered and (b) quenched samples at 25 °C and inset contains the corresponding electric circuit model used for fitting the impedance data.

these materials obeys the power law; $\sigma(\omega)\,\alpha\,\omega^{n}$ with a slope change governed by n. This law is associated with dynamic of hopping conduction process. Various physical processes are also associated with n (exponent). When $n \geqslant 1$, the charge carriers hopping can be associated with the translational motion and when $n \leqslant 1$, charge carriers hopping can be localized.

Here, as the DC conductivity part (σ_{dc}) is not present, the AC conductivity part $\sigma_{ac}(\omega)$ can be explained as, $\sigma_{ac}(\omega) = A\omega^{n}$ [17]. In the graph, the variation of log (σ_{ac}) and log (frequency) at room temperature plots show the existence of two dissimilar conduction mechanisms as the slope varies with frequency.

3.4. Complex Impedance Spectroscopy

Impedance spectroscopy shed light upon the electrical characteristics of the polycrystalline sample. This method distinguishes between the intrinsic (grain), extrinsic (grain boundary) and sample electrode interface contributions to the electrical properties of the material [18]. Figure 5 depicts the Nyquist plot of both the (a) sintered and (b) quenched samples. It is seen that for the sintered sample only contribution of grain effect is observed and the electrical model used to fit the impedance data is RQC (i.e. R = resistor, Q = constant phase element, C = capacitance). Further it is seen that for the quenched sample, the electrical model used is RQC-RC suggesting both the grain and grain boundary association.

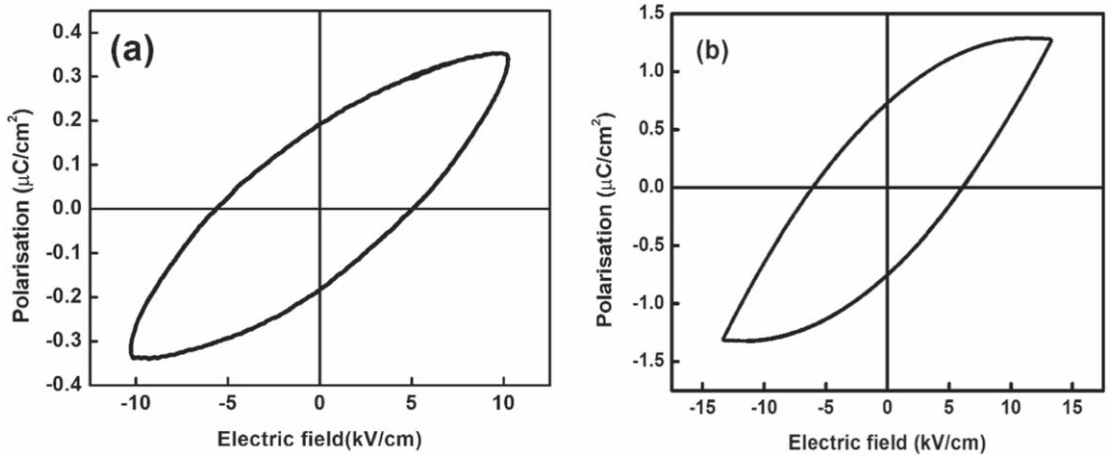

Figure 6. Room temperature polarisation versus electric field for (a) sintered and (b) quenched samples.

3.5. Ferroelectric properties

The measurements of P-E hysteresis loop depict the existence of the loop together with the reversal of spontaneous polarization on application of electric field. Figure 6 shows the electric field versus polarization of both (a) sintered and (b) quenched samples at room temperature. Ferroelectric hysteresis loops were traced by employing P. E. loop Tracer (Marine India) comprising of modified Sawyer Tower circuit at room temperature and operating at 50 Hz. The P-E loop Tracer has integrated parts like PC, Software, programmable voltage source (up to 5 kV), silicon oil bath and oven. The electric field is calculated by dividing the voltage by the thickness ($E = V/d$) across the sample by measured thickness. The horizontal *x*-axis represents the magnitude of the field applied. The sample is then coupled in series with a parallel RC circuit, which compensates phase shift owing to dielectric loss or conductivity in the synthesised sample. It is observed as the samples are quenched from sintered state, a typical ferroelectric P-E loop is depicted. The remnant polarization for sintered and quenched samples is 0.065 and 1.067 μc cm^{-2}respectively. As achievable domain alignment occurs in quenched samples so higher value of remnant polarization is observed than the sintered samples. The coercive field for sintered and quenched samples is 0.016 and 4.576 kV cm^{-1} respectively.

3.6. Excitation performance

The excitation performance of both sintered and quenched samples are depicted in figure. The sintered and quenched samples were at first electrode with silver paint on both opposite sides which is further annealed at 120 °C for 4 h to remove moisture. Then copper wires were soldered onto the parallel surface of the both sintered and quenched samples. Further the sample acted as a parallel plate capacitor which is connected in series with a function generator, resistor (1000 Ohm) and a digital signal oscilloscope. The electric field applied from the function generator was constant (10 V_{p-p}) for both sintered and quenched samples. It is observed that with frequency sweep from 100 kHz to 30 MHz the output voltage first rise attains a peak and then declines in figure 7 (a: sintered), (b: quenched). The resonance phenomena are realized and the maximum voltage obtained for sintered and quenched samples are 116 mV at 5000 kHz and 160 mV at 4500 kHz respectively.

4.Conclusion

The structural and microstructure of sintered and quenched sample of Al_2O_3 doped fused silica samples were investigated. The dielectric properties depict high dielectric constant and low loss. The impedance spectroscopy revealed at room temperature only the assistance of grains. The constant electrical field was applied to realize the sample excitation performance experimentally by a circuit design. The fabricated samples can be utilized in series RC filter circuits as per the obtained experimental results.

ORCID iDs

Sugato Hajra https://orcid.org/0000-0002-2049-4509
Manisha Sahu https://orcid.org/0000-0003-0175-7606
Varsa Purohit https://orcid.org/0000-0002-4614-4590

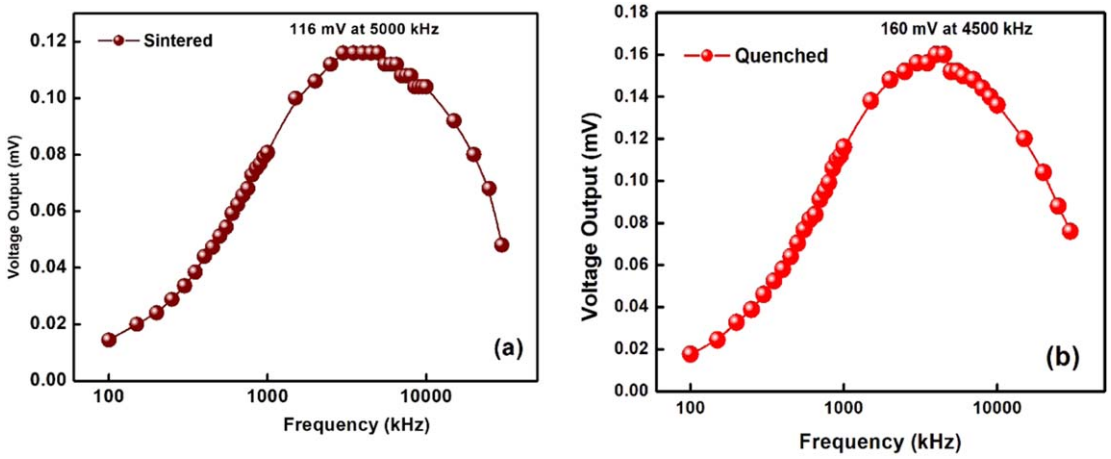

Figure 7. Excitation performance of the (a) sintered and (b) quenched samples under the constant electric field at room temperature.

References

[1] Thao P N, Yoshida S and Tanaka S 2018 *Micromachines* **9** 455
[2] Kumar A, Kim S H, Peddigari M, Jeong D-H, Hwang G-T and Ryu J 2019*Ryu Electronic Materials Letters* **15** 323
[3] Lonkar C M, Premkumar S, Kharat D K, Kumar H H, Sahab Prasad and Balasubramanian K 2013 *Journal of Materials Science: Materials in Electronics* **24** 1989
[4] Wani A L, Ara A and Usmani J A 2015 *InterdiscipToxicol.* **8** 55
[5] Saito Y, Takao H, Tani T, Nonoyama T, Takatori K, Homma T, Nagaya T and Nakamura M 2004 *Nature* **432** 84
[6] Wan W, Feng Y, Yang J, Bu W and Qiu T 2016 *Ceramics International* **42** 6436
[7] Sahu M, Hajra S, Mohanta K, Purohit V and Choudhary R N P 2019 *SN Applied Sciences* **1** 1254
[8] Hajra S, Mohanta K, Sahu M, Purohit V and Choudhary R N P 2019 *Applied Physics* A **125** 369
[9] Hajra S, Sahu M, Purohit V, Panigrahi R and Choudhary R N P 2019 *Materials Research Express* **6** 096319
[10] Koops C G 1951 *Phys. Rev.* **83** 121
[11] Uniyal P and Yadav K L 2009 *J. Phys.: Condens. Matter* **21** 405901
[12] Purohit V and Choudhary R N P 2019 *Applied Physics* A **125** 125
[13] Kim T Y, Kim S K and Kim S-W 2018 *Nano Convergence* **5** 30
[14] Panigrahi R, Hajra S, De M, Kumar A, James A R and Choudhary R N P 2019 *Solid State Sciences* **92** 6–12
[15] James A R and Srinivas K 1999 *Mater. Res. Bull.* **34** 1301
[16] Rouahi A, Kahouli A, Challali F, Besland M P, Vallée C, Yangui B, Salimy S, Goullet A and Sylvestre A 2013 *J. Phys. D: Appl. Phys.* **46** 065308
[17] Dhahri Ah, Dhahri E and Hlil E K 2018 *RSC Adv.* **8** 9103
[18] Lin Y, Yang H and Zhu Z 2012 *Materials Chemistry and Physics* **136** 286